Eur. Phys. J. E **6**, 277–285 (2001)

THE EUROPEAN PHYSICAL JOURNAL E

EDP Sciences

Structure and frustration in liquid crystalline polyacrylates I. Bulk behaviour

B.I. Ostrovskii[1,2], S.N. Sulyanov[2], N.I. Boiko[3], V.P. Shibaev[3], and W.H. de Jeu[1,a]

[1] FOM-Institute for Atomic and Molecular Physics, Kruislaan 407, 1098 SJ Amsterdam, The Netherlands
[2] Institute of Crystallography, Academy of Sciences of Russia, Leninsky pr. 59, Moscow, 117333 Russia
[3] Moscow State University, Department of Chemistry, Moscow, 119899 Russia

Received 28 February 2001 and Received in final form 6 August 2001

Abstract. The phase behaviour and structure are reported of a new type of frustrated side-chain liquid crystalline (LC) polymer, a polyacrylate with phenylbenzoate mesogenic side groups and a narrow polydispersity. At a high degree of polymerisation the LC polymers show a nematic, a smectic-A_d, a re-entrant nematic and a $\tilde{C}$ phase, for shorter chains only a nematic and a $\tilde{C}$ phase. This constitutes a new example of nematic re-entrance for which the driving field is the length of the polymer chain. The smectic-A_d layers consist of partially overlapped side groups while in the $\tilde{C}$ phase the side chains are rearranged into chevron-like blocks of bilayers. We propose an explanation of the frustrated phase behaviour in terms of these two different competing length scales and their coupling to the backbone conformations.

PACS. 64.70.Md Transitions in liquid crystals – 78.70.Ck X-ray scattering – 61.30.Eb Experimental determinations of smectic, nematic, cholesteric, and other structures

1 Introduction

In side-chain liquid crystalline (LC) polymers hydrocarbon spacers link mesogenic moieties to a polymer chain. These materials possess a unique combination of LC ordering and specific polymer properties. They have received increasing attention because of the interest from a fundamental point of view as well as due to their technological potential in areas as information storage, nonlinear optics and aligning coatings for display applications [1]. Flexibility of the backbone chain as well as of the spacer is essential to give the mesogenic cores enough freedom to self-assemble into LC phases [2]. However, the coupling between the main-chain conformation and the LC ordering field restricts this freedom. From small-angle neutron scattering [3], the main-chain conformations are found to deviate from a three-dimensional (3D) Gaussian random coil into prolate or oblate shapes [4]. In particular, smectic ordering leads to a conflict between the tendency of the backbone toward maximizing the internal entropy and the smectic field confining it in 2D. This intrinsic competition distinguishes LC polymer smectics from their monomeric counterparts and affects the delicate balance between nematic and smectic ordering [5,6].

Liquid crystalline polyacrylates with phenyl benzoate side groups are known to form nematic (N) and various smectic mesophases [1,2,7]. Recently, some remarkable new features have been observed in the phase behaviour of monodisperse LC polyacrylates in comparison to the same polydisperse materials [8]. For the monodisperse samples, upon increasing the length of polymer chain (degree of polymerisation P_w) a smectic-A_d (Sm-A_d) phase appears (see Fig. 1), which is not observed in the polydisperse material. This Sm-A_d phase becomes unstable on cooling and melts into a re-entrant nematic (RN) phase. Upon further cooling a $\tilde{C}$ phase is formed which has a 2D monoclinic lattice. The phase diagram shows a particular point, the so-called re-entrant point (RP) that allows passing from the N to the RN phase in a continuous way. This unique case of nematic re-entrance is only found for highly fractionated polymer material.

Re-entrancy is observed in a broad range of materials usually referred to as frustrated systems. Examples include magnetic spin glasses [9], surface adsorbates [10] and liquid crystals [11,12]. Since the discovery by Cladis [11], in a large number of LC compounds and mixtures single and multiple nematic re-entrances have been observed [12]. The common feature of these materials is a Sm-A lattice spacing incommensurate with the length of a single molecule. Nematic re-entrancy is often found for molecules with strongly polar terminal groups (CN or NO_2), but has also been reported for sterically strongly asymmetric mesogens [13] and for mixtures of a side-chain LC polymer with a low-molecular mass nematic [14]. In all these cases the smectic layer structure is destroyed and the less ordered nematic phase appears due to the

[a] e-mail: dejeu@amolf.nl

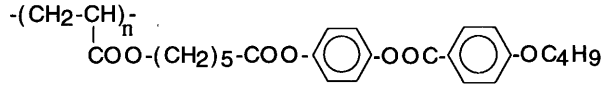

PABB-5

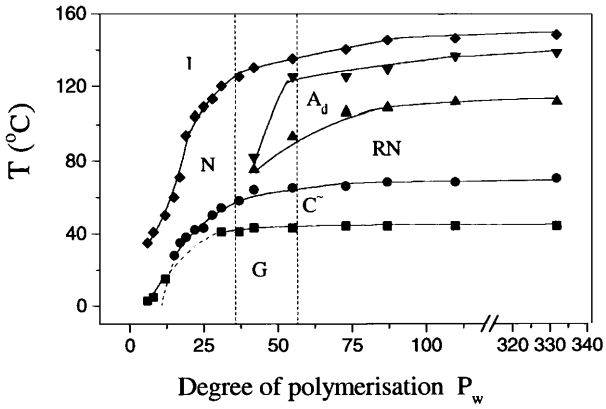

Fig. 1. Structural formula and phase diagram of the liquid crystalline polyacrylate PABB-5.

frustration induced by competing order parameters that favour different periodicities [15–17]. Alternatively, the frustration might be relieved by the formation of a phase with 2D periodicity [16]. Because of the rather poor understanding of the microscopic interactions responsible for smectic ordering in LC polymers, identifying the competing order parameters that account for the N–Sm-A_d–RN behaviour in LC polyacrylates is not obvious. In the absence of strongly polar terminal groups, dipolar frustration [12,16,17] cannot play an important role. The phase diagram of Figure 1 indicates that the frustrated behaviour in LC polyacrylates is probably driven by changes of the polymer backbone conformation, which become more pronounced for long chains.

In this paper we present a study of the structure and phase behaviour of the new re-entrant LC polyacrylate system. Emphasis will be on the vicinity of the re-entrant point where the Sm-A_d layering ceases to be stable. X-ray diffraction (XD) has been used to characterize the bulk structure. It provides information about the symmetry of the LC phases and the positional correlations along and perpendicular to the mesogenic side groups. As expected, the layers in the Sm-A_d phase are formed by partially overlapping side groups, providing an interlayer spacing incommensurate with respect to the length of a mesogen. In the $\tilde{C}$ phase a 2D oblique lattice of the side chains is formed, which are arranged in chevron-like blocks of bilayers. The $\tilde{C}$ phase has a two-dimensional monoclinic lattice and retains liquid-like order in the third direction. This structure is similar to the so-called ribbon phase in terminally polar mesogens [12,18]. The local structure of the nematic and RN phase is characterized by diffuse peaks at positions characteristic of the lattice parameters of the Sm-A_d and $\tilde{C}$ phase, respectively. We propose an explanation of the structural changes in LC polyacrylates in terms of a coupling between the smectic ordering of the side groups and the polymer backbone conformation. In an accompanying paper we discuss thin films of the same material. In this situation additional effects of the surface curvature come into play, as evidenced by a nanometer-size lateral periodicity at the air-film interface.

Table 1. Influence of different polydispersities on the phase behaviour of PABB-5 for $P_w = 160$ (temperatures in °C; G and I stand for the glassy and the isotropic phase, respectively).

$\overline{M}_w/\overline{M}_n = 2.9$	G 28 $\tilde{C}$ 70 N 138 I
$\overline{M}_w/\overline{M}_n = 1.16$	G 44 $\tilde{C}$ 68 RN 108 Sm-A_d 129 N 145 I

2 Experimental

The LC polyacrylates with phenyl benzoate mesogenic groups (PABB-5, Fig. 1) were synthesized and fractionated into highly monodisperse samples as described in [8]. The degree of polymerisation is defined by $P_w = \overline{M}_w/M_0$, where $\overline{M}_w$ is the weight-average molar mass of the polymer and M_0 the monomer mass. The polydispersity is given by $\overline{M}_w/\overline{M}_n \approx 1.1$, in which $\overline{M}_n$ is the number-average molar mass of the polymer. As the polydispersity is close to one, to a good approximation $P_w \approx n$, the number of monomers per chain. The importance of the molecular mass distribution on the phase behaviour [1, 2,19] is demonstrated in Table 1 for two samples with $\overline{M}_w \approx 4 \times 10^4$ and different polydispersity.

The nature of the phases was identified by XD with CuK_α radiation (wavelength $\lambda \approx 0.154$ nm) using two different types of set-up. For the KARD diffractometer with 2D-detector described in [20], the incident beam is monochromatised by a graphite crystal and collimated by pinholes. Defining the wave vector transfer $q = (4\pi/\lambda)\sin\theta$, where θ is the scattering angle, at a sample-detector distance of 0.8 m the resolution in the scattering plane is about $\Delta q \approx 0.1$ nm^{-1} (full width at half-maximum, FWHM). Measurements at higher resolution were made with a triple-axis diffractometer at an 18 kW rotating anode generator (Rigaku RU-300H) [21]. The incident beam was monochromatised and focused in the direction perpendicular to the scattering plane using a bent graphite (002) crystal. The scattering geometry is shown in Figure 2. We define q_z as the component of the wave vector transfer parallel to the nematic director **n** (aligned parallel to a magnetic field H of 1 T) and $q_\perp$ as the perpendicular component. The resolution along q_z as defined by pre-sample and pre-detector slits was found to be Gaussian with $\Delta q_z \approx 0.04$ nm^{-1}. The LC polymer was placed in a sealed thin-wall glass capillary with a diameter of 1.5 mm and inserted in a two-stage oven providing temperature stability within 0.1 °C.

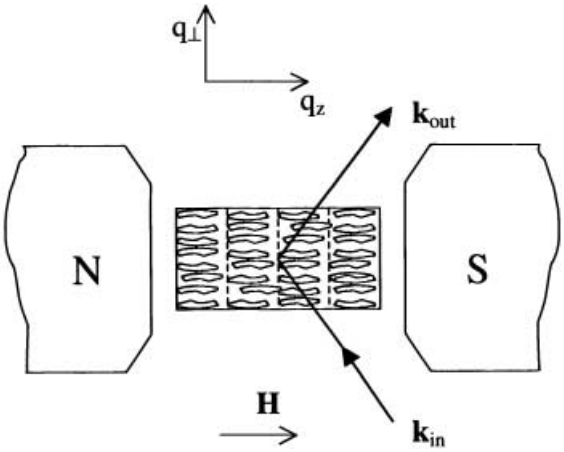

Fig. 2. Scattering geometry with magnetic field direction and wave vector transfer components q_z and $q_\perp$.

3 Results

The coordinates of the re-entrant point in the T-P_w phase diagram have been determined as $P_w(\mathrm{RP}) = 42$ and $T(\mathrm{RP}) = 74\,^\circ\mathrm{C}$. Samples corresponding to P_w values of 31, 37, 55 and 110 have been studied (compare Fig. 1). For $P_w = 55$ the diffraction patterns in the high-temperature nematic phase exhibit in the small-angle region diffuse spots along the direction of the magnetic field at $q_z \approx 1.8$ nm^{-1}, corresponding to an average distance of about 3.5 nm along **n**. In addition diffuse outer halos are found in the equatorial direction at $q_\perp \approx 14$ nm^{-1}, indicating an average distance between the side chains of the order of 0.46 nm. Evidently, the mesogenic side groups are oriented parallel to the field and the sample possesses uniaxial symmetry around **n**. Cross-sections of the diffuse halos can be well fitted by a Lorentzian lineshape $[1+\xi_\perp^2(q_\perp - q_{\perp 0})^2]^{-1}$ (see Fig. 3a). For the corresponding transverse correlation length we find $\xi_\perp \approx 0.8$ nm.

With DSC no heat effects are detected at the N–Sm-A_d and Sm-A_d–RN transitions [8]. However, conclusive evidence can be obtained from the XD data depicted in Figure 4 for $P_w = 55$. All transitions were found to be completely reversible upon temperature cycling. The transition from the nematic to the Sm-A_d phase is indicated by the appearance of sharp inner reflections in the small-angle region (Fig. 4a). These reflections form a set of $(00m)$ peaks at $q_{zm} = 2\pi m/d$, where m is an integer and d the smectic layer spacing, which is practically temperature independent ($q_{z1} = 1.78$ nm^{-1}). The second and third harmonics have intensities of about 70% and 1% of the value of the first-order peak. The interlayer spacing $d = 3.53$ nm considerably exceeds the length $L \approx 2.6$ nm of a side group in the all-trans configuration. Hence the mesogenic side groups, being orthogonal to the smectic planes, partly overlap each other giving rise to a Sm-A_d structure. The longitudinal peaks along q_z were found to be resolution limited. They perfectly reproduce the Gaussian shape of the resolution function (see Fig. 5a). Hence their width is determined by finite smectic domains [22], the average size of which can be estimated using the Scherrer formula as

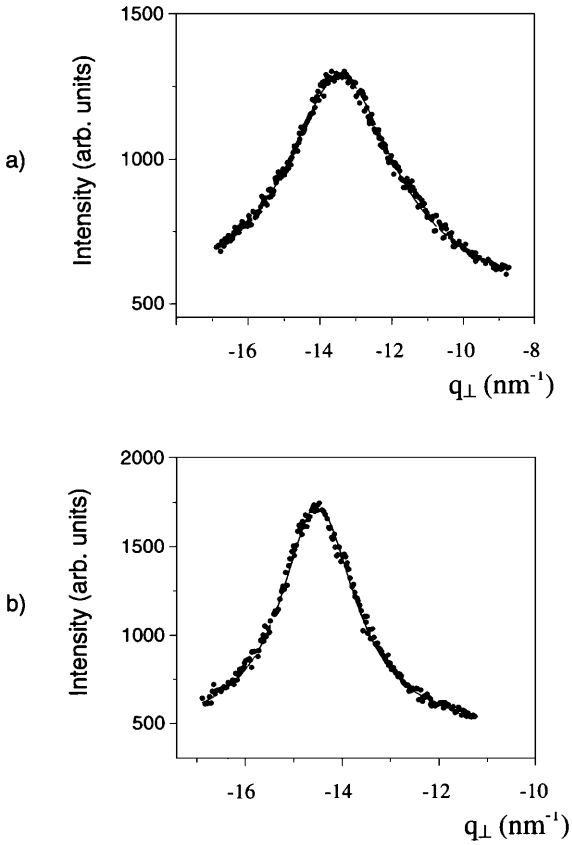

Fig. 3. X-ray intensity profile along $q_\perp$ for $P_w = 55$. (a) High-temperature nematic phase ($T = 126\,^\circ$C). (b) $\tilde{C}$ phase ($T = 55\,^\circ$C). Solid lines represent a Lorentzian fit.

$R \approx 2\pi/\mathrm{FWHM} \approx 150$ nm. This corresponds to about 40 smectic layers. The mosaicity as determined from rocking curves is typically 2°. In the wide-angle region the diffuse halos have nearly the same position and width as in the nematic phase. Thus the packing of mesogenic side groups within the smectic planes is still liquid-like.

For $P_w = 55$ the Sm-A_d phase is stable between 125°C and 91 °C. With decreasing temperature the maximum of the smectic peak intensity is reached around 110-120 °C; then the intensity diminishes, though the peak remains resolution limited. A broadening of this longitudinal peak identifies the RN–Sm-A_d phase transition at 91 °C. This broadening signals the absence of a long-range smectic density modulation. In the RN phase fluctuational Sm-A_d order is still observed in a temperature range of about 2 °C below the phase transition. In the RN phase the mesogenic side chains are again aligned by the magnetic field, but just below the phase transition the mosaic is as large as 10° (FWHM).

At much lower temperatures in the RN phase a quite different diffuse scattering pattern is observed (Fig. 4b). Three diffuse peaks develop with an angular width along q_z corresponding to positional correlations of the order of $\xi_\parallel \approx 5$–9 nm. The incommensurate peak positions are close to the lattice parameters of the low-temperature $\tilde{C}$ phase. With decreasing temperature the diffuse peaks

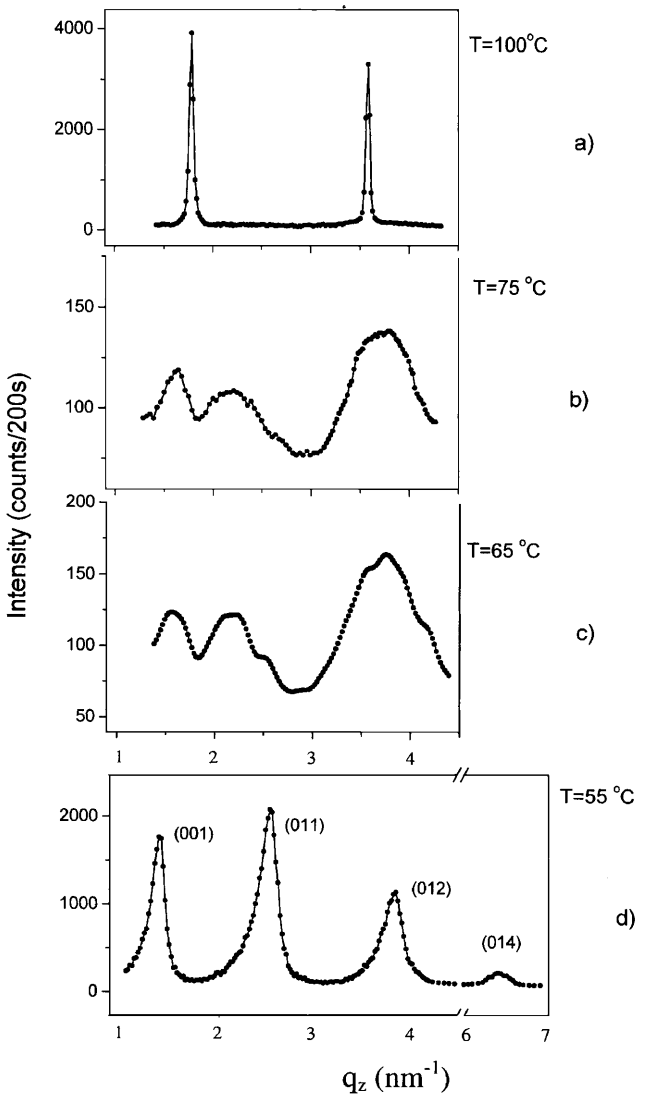

Fig. 4. X-ray diffraction pattern at small scattering angles of an aligned sample with $P_w = 55$. (a) Sm-A_d phase. (b, c) Re-entrant nematic phase well below the Sm-A_d–RN phase transition; the data have been smoothed for clarity. (d) $\tilde{C}$ phase with peaks indexed on a 2D monoclinic unit cell.

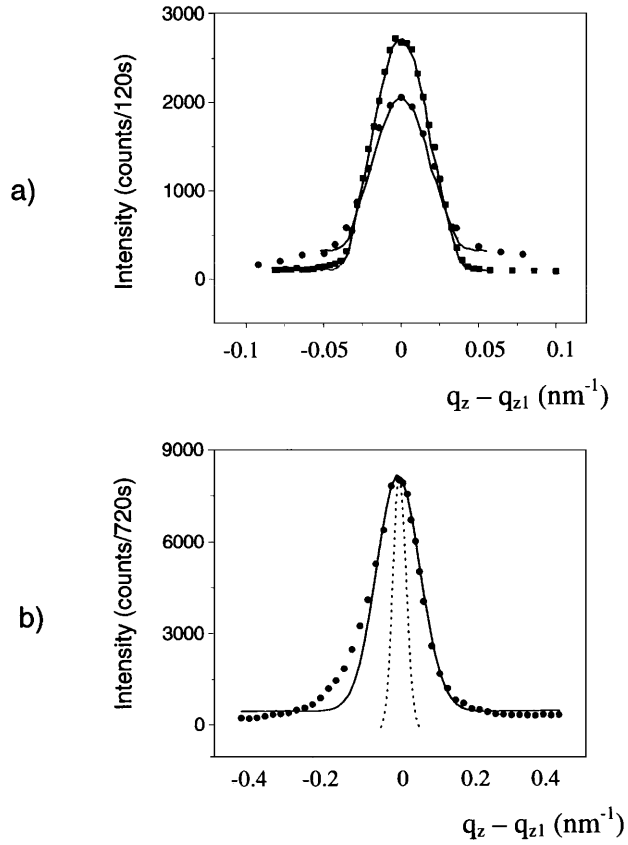

Fig. 5. X-ray line profiles and instrumental resolution for an aligned sample with $P_w = 55$. (a) Sm-A_d phase ($T = 118\,^\circ$C); squares and circles correspond to first and second Bragg peak, respectively; solid lines indicate the resolution. (b) (001) peak in the $\tilde{C}$ phase ($T = 55\,^\circ$C). Filled circles indicate data points, the solid line is a Gaussian fit, while the dotted curve gives the resolution function. The asymmetry of the peak at the low-q side is due to the relatively poor mosaicity of the sample.

sharpen and become more intense, signalling an increase of the scale of the $\tilde{C}$-like fluctuations, see Figure 4c. Upon further cooling down, the phase transition from the RN to the $\tilde{C}$ phase is indicated by a condensation of the diffuse spots to sharp $(0km)$ peaks (k and m integer, Fig. 4d). These peaks cannot be attributed to a smectic layer periodicity only and have to belong to some type of 2D or 3D lattice. The positions of the wide-angle diffuse halos now correspond to about 0.44 nm and the transverse correlation length has increased somewhat to $\xi_\perp = 1.3$ nm (see Fig. 3b). Hence the positional correlations between the side chains are still short range: in the $\tilde{C}$ phase the positional ordering is liquid-like in one direction (defined here as the x-direction). At the transition to the $\tilde{C}$ phase the mosaicity was found to be large (10-20°). This is similar to the situation in the RN phase, in spite of starting from well-aligned samples in the Sm-A_d phase. For such nearly powder-averaged samples all the characteristic peaks of the $\tilde{C}$ phase show up in just one scan (compare Fig. 4). However, this does not help to establish the symmetry of the 2D lattice. By cycling through the transition temperature we found that the best mosaic spread of 4–6° was achieved by leaving the sample for 10–12 hours in a strong magnetic field at the RN-$\tilde{C}$ phase transition region ($\sim 59\,^\circ$C). Contour plots of the 2D diffraction data for such an aligned sample are shown in Figure 6. The first two diffraction peaks have as coordinates (q_y, q_z) in nm^{-1} (0, 1.42) and (1.51, 2.09), respectively. The angle between the corresponding reciprocal space vectors is about 36°. The 2D unit cell of the $\tilde{C}$ phase appears to be monoclinic and can be described by basis vectors **a** and **b** and their mutual angle γ. Such a structure gives rise to (001) (010), (011) and other combined reflections of the type $(0km)$, see Figure 7. The first two reflections can be indexed either as (001) and (010) or as (001) and (011). Of course, the real space lattice will be the same in both

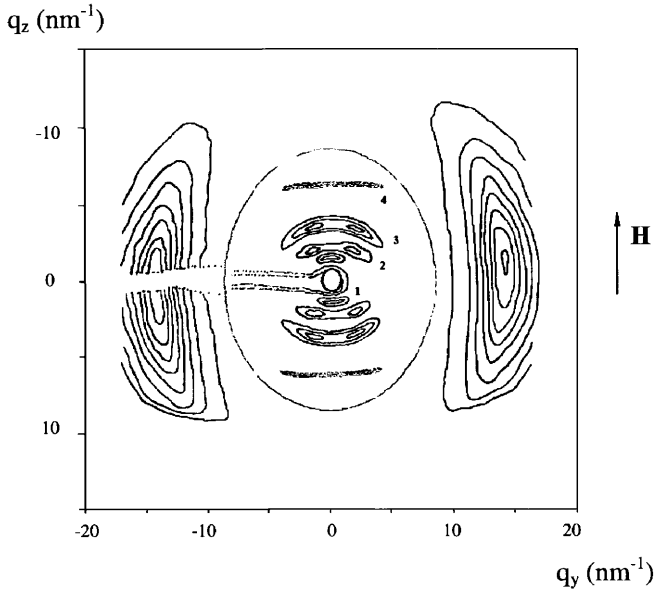

Fig. 6. Equal-intensity contours in the q_z-q_y plane for an aligned sample with $P_w = 55$ in the $\tilde{C}$ phase ($T = 55\,^\circ$C); q_z and (q_x, q_y) are defined along and perpendicular to the director, respectively; q_x is along the "liquid" direction (see text). The spots 1-4 are indexed on a 2D monoclinic unit cell as (001), (011), (012) and (014).

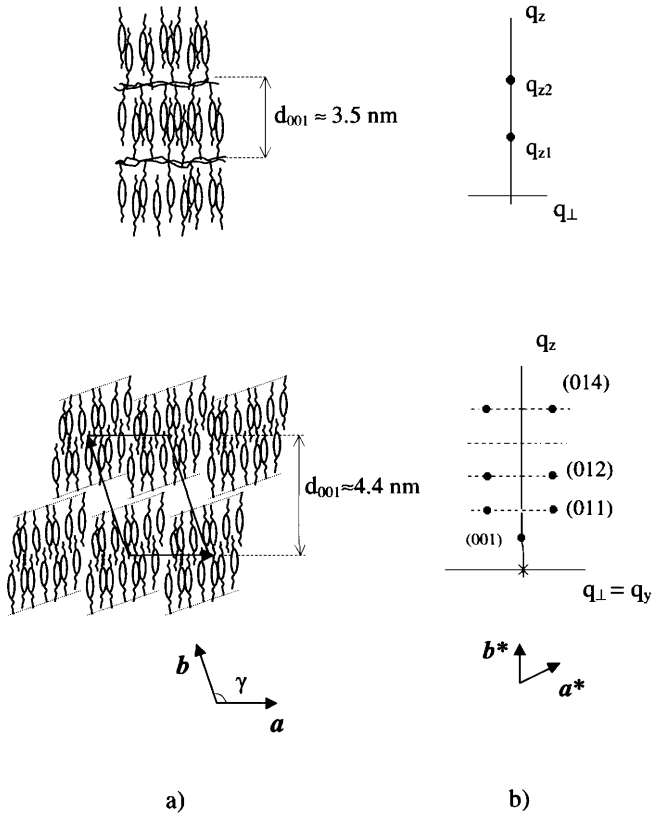

Fig. 7. (a) Schematic representation of the real space structure of the Sm-A_d phase (upper part) and $\tilde{C}$ phase (lower part) and (b) the corresponding diffraction patterns (half reciprocal space only). The lamellar spacing in the Sm-A_d phase is ~ 3.5 nm. In the $\tilde{C}$ phase the side groups of the LC polymer are arranged in chevron-like blocks of bilayers, which are packed in a 2D monoclinic lattice; the bilayer spacing is ~ 4.4 nm. The structure is liquid-like perpendicular to the lattice plane drawn.

cases. In agreement with standard crystallographic rules, we choose the second set of indices, which corresponds to the primitive unit cell of a monoclinic lattice with the smallest parameters and the angle γ closest to 90°. This leads to reciprocal space vectors defined as $\mathbf{b}^* = (0, 0, 1)$ and $\mathbf{a}^* + \mathbf{b}^* = (0, 1, 1)$. These vectors may be inverted to give the basis vectors $\mathbf{a}$ and $\mathbf{b}$ of the real space lattice: $a = 1/(a^* \sin\gamma)$ and $b = 1/(b^* \sin\gamma)$. The corresponding monoclinic unit cell parameters are $a = 4.16$ nm, $b = 4.86$ nm, $\gamma = 114°$ (compare Fig. 7).

The equatorial arrangement of the wide-angle diffuse halos in the $\tilde{C}$ phase is essentially the same as in the N and RN phases. Hence in all phases the director $\mathbf{n}$, associated with the average orientation of the long axes of the side groups, is effectively fixed along the direction of the magnetic field. The degeneration of the vector $\mathbf{a}^*$ around $\mathbf{n}$ duplicates primary spots of the type (011), (012) and (014), which corresponds to the formation of a texture with q_z as symmetry axis (compare Fig. 6). The symmetry of the 2D lattice leads to a model in which the structural elements are centred at the points of the monoclinic translation lattice (see Fig. 7). As $\mathbf{b}^*$ is parallel to the symmetry axis of the lattice, the appropriate structural elements are blocks of bilayers of the side groups with a length $1/b^* = 4.43$ nm. Because the length of a mesogenic side group is about 2.6 nm, the end alkylene moieties partly overlap within these bilayers. Moreover, in such a structure the side chains may be tilted relative to the local "layer", thus forming chevron-like blocks [12,18] (see Fig. 7). Finally, we note that some reflections allowed by the symmetry of the $\tilde{C}$ lattice are not observed experimentally, for example (002), (010) and (013). This may be attributed to peculiarities of the form factor of the scattering units responsible for the 2D density modulation.

Contrary to the Sm-A_d peak, the ($0km$) diffraction peaks in the $\tilde{C}$ phase are not resolution-limited (see Fig. 5b). They can be well fitted by a Gaussian lineshape. As a starting point we attribute this line broadening to the effect of finite domain sizes. Then the peak profile is a convolution of the Gaussian instrumental resolution with the Fourier transform of a box-function of width R: $F(q_z) = \sin^2(Rq_z/2)/(q_z/2)^2$. The latter function can be well approximated by a Gaussian of the same FWHM, and the convolution results again in a Gaussian profile as experimentally observed. The deconvolution of the experimental profile with the known resolution function results in an average domain size of about 60 nm. Evidently, the 2D periodic structure in the $\tilde{C}$ phase is strongly defective. Alternatively, the line broadening could be attributed to a limited range of the positional correlations in the system. Then the density-density correlation function will decay like $g(r) \sim r^{-1}\exp[-r/\xi]$, where ξ is the

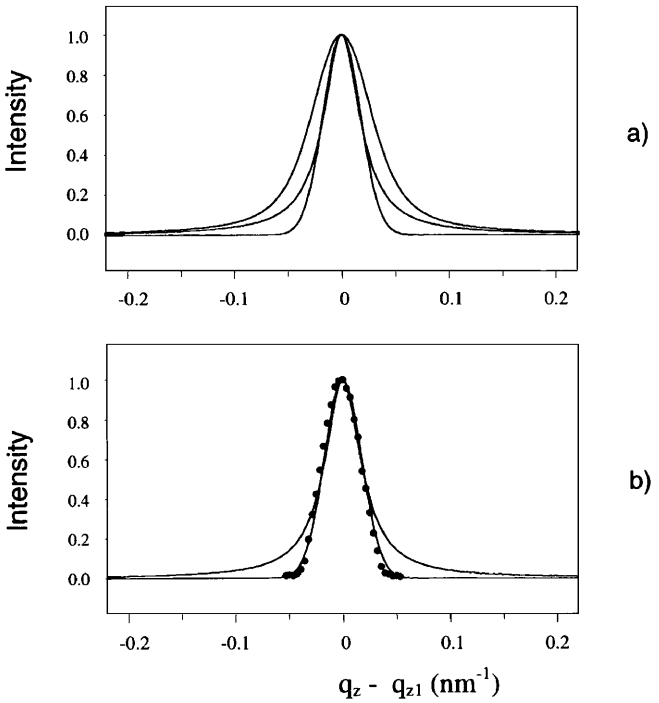

Fig. 8. Comparison of Gaussian and Lorentzian diffraction profiles. (a) Simulation of the resolution broadening of a Lorentzian lineshape. From inside to outside: Gaussian profile, Lorentzian of the same FWHM, convolution of the two. (b) Experimental resolution function of the diffractometer (filled circles), fitted to a Gaussian and compared with a Lorentzian of the same width.

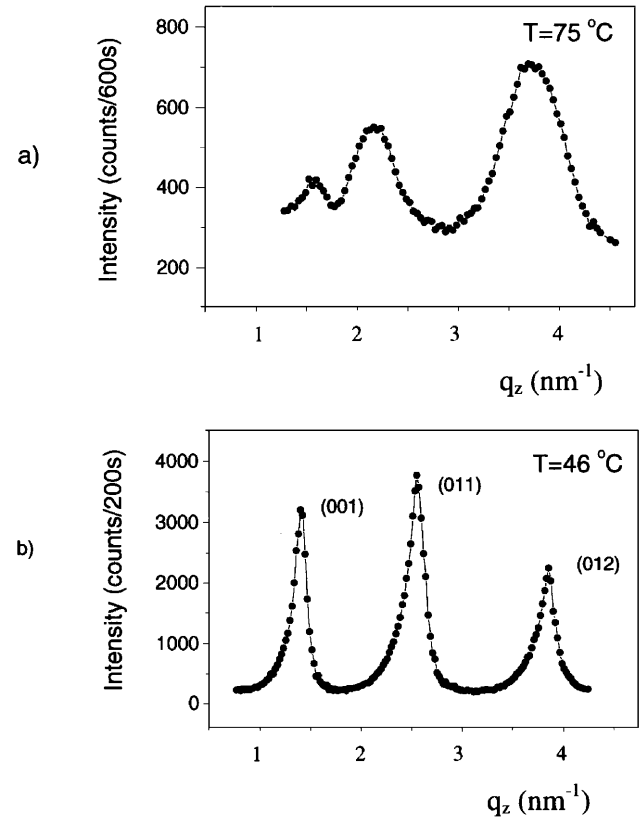

Fig. 9. X-ray diffraction patterns at small angles for $P_w = 37$. (a) Nematic phase; (b) $\tilde{C}$ phase. The peaks are indexed on a 2D monoclinic unit cell as before.

correlation length and the Fourier transform yields a Lorentzian structure factor $S(q) \sim 1/(\xi^{-2} + q^2)$. The convolution of a Gaussian resolution function with a Lorentzian structure factor gives a lineshape with "long tails" of the Lorentzian type. As demonstrated in Figure 8, this situation can be easily distinguished from a Gaussian lineshape. Thus, we conclude that for the $\tilde{C}$ phase of the LC polyacrylates the XD line broadening is due to finite domain sizes.

Figure 9 displays diffraction data for the LC polyacrylate with $P_w = 37$. In this case the phase diagram shows no intermediate Sm-A_d phase and nematic transforms directly to the $\tilde{C}$ phase. Interestingly, the diffuse spectra in the nematic phase show $\tilde{C}$-like fluctuations at temperatures far above the N-$\tilde{C}$ phase transition region. A crossover from $\tilde{C}$-dominated fluctuations to Sm-A_d–type local ordering occurs only above 95 °C. Even at temperatures around 75 °C, which is closest to P_w(RP), there are no indications of Sm-A_d fluctuations (Fig. 9). The transition to the $\tilde{C}$ phase occurs at 55 °C. The parameters of the corresponding 2D monoclinic lattice differ less than 1% from that described above for $P_w = 55$.

4 Discussion

The phase diagram presented in Figure 1 manifests frustrated behaviour in dependence on the length of the polymer chain. Below $P_w = 42$, a nematic phase is found; above this point, a Sm-A_d phase is inserted. This Sm-A_d layering becomes unstable upon cooling and melts into a re-entrant nematic phase. In all cases at low temperatures the $\tilde{C}$ phase is formed. Evidently the length of the polymer chain and thus its conformational freedom plays an essential role. Before attempting to give a microscopic picture, we note that the general shape of the phase diagram of Figure 1 can in principle be described by extending the phenomenological model of Pershan and Prost [23] for low-molecular mass frustrated smectics. They model the re-entrant phase diagram in terms of a coupling between the smectic ordering field ψ and an external variable like pressure or the concentration of a binary mixture. In our case the driving field for re-entrant behaviour would be the length of the polymer chain n. Different contributions to the free-energy density can be distinguished: the backbone entropy, the side group interaction, and the coupling between them. The cross term describing the coupling of ψ with external variables like the length n of the polymer chain and the density of the polymer ρ, can be presented in its simplest form as $g(n, \rho)\psi^2$. This allows deriving an expression for the total free energy that gives rise to a phase diagram with a re-entrant point after expanding g in a power series in $(\rho - \rho_0, n - n_0)$. The problem with this approach is that there is no real clue how to choose ρ_0 and n_0, the "optimum" density and degree of polymerisation.

Microscopically, the type of frustrated behaviour shown in Figure 1 requires a description based on order parameters with associated competing length scales [16]. Because the mesogenic units in LC polyacrylate have no strongly polar terminal groups, such behaviour is not expected to originate from dipolar frustration that determines re-entrant phase diagrams of conventional terminally polar mesogens [15–17]. From the experiments, the competing lengths in the system result from differently overlapping mesogenic side chains. The first length is about 3.5 nm and determines the layer spacing in the Sm-A_d phase. The second one (∼4.4 nm) corresponds to "almost bilayers" of side chains. It exists on a local scale in many nematic regions of the phase diagram and condenses in the $\tilde{C}$ phase. We postulate that the corresponding minima in the free energy are comparable and separated by only a small-energy barrier. Consequently, minor additional interactions in the system might induce a transition from one minimum to another. In this model the driving force for structural transformations originates from a coupling between changes in the backbone conformation (depending on P_w) and the smectic ordering field.

In contrast to their low molecular mass counterparts, polymeric liquid crystals have an intrinsic conflict between the drive of the backbone to adopt a random coil conformation and the ordering tendency (orientational and smectic layering) associated with the mesogenic side groups. To obtain macroscopic LC behaviour a flexible spacer is required to decouple to the right extent these different tendencies. The actual conformation of the backbone can be determined with small-angle neutron scattering (SANS) of selectively deuterated samples [3, 4]. The coil formed by the backbone has an anisometric shape, which can be expressed by the main components of the radius of gyration tensor: $R_{g\parallel}$ and $R_{g\perp}$. The mean square of the radius of gyration was found to be proportional to the degree of polymerisation [4,24], in agreement with a model of freely joined chains. SANS results on several nematic polyacrylates indicate that the backbone preferably adopts a weakly prolate shape ($R_{g\parallel} > R_{g\perp}$, *i.e.* the average direction of the backbone is parallel to **n**). These observations have been confirmed by NMR studies of LC polyacrylates [25]. However, less flexible LC polymethacrylates with the same side chain and spacer length tend to coil up in the nematic phase in an oblate configuration (side chains preferably perpendicular to the backbone).

In the smectic phase the backbones of both acrylates and methacrylates usually adopt an oblate arrangement and are to some extent confined between the sublayers of the mesogenic cores [4]. Long chains seem to be more strongly confined than short ones [24]. Various types of description of the chains (Gaussian, rod-like and self-avoided walk) give nearly the same anisotropy ratio $R_{g\parallel}/R_{g\perp}$ [5]. In a smectic phase a confined backbone can cross a mesogenic sublayer creating a local distortion of the smectic layering. A typical distance between two adjacent side chains along a backbone (say ∼0.5 nm) is factor of six smaller than a typical layer spacing. This implies that for an oblate configuration about six side chains do not fit into the smectic lamellae during one crossing event. Hence in this situation one would expect that a sufficiently large density of crossing defects would induce melting of the smectic layers [5].

Particularly relevant to the present series of LC polyacrylates is a SANS study of a LC polyacrylate with cyano-terminated side groups [4], which shows with decreasing temperature a phase sequence N–Sm-A_d–RN. The results indicate an oblate backbone conformation in the N and Sm-A_d phases, which transforms to prolate in the RN phase. Quasi-elastic neutron scattering supports this interpretation [26]. Additional X-ray measurements show that the associated change in backbone conformation takes place in a small pre-transitional Sm-A_d region in the RN phase [27]. Though distinct from these cyano-terminated polycrylates, whose phase behaviour is determined by dipolar frustration, we postulate for the present PABB-5 series the same type of conformational changes. This would mean that the polyacrylate main chain rather than the specific origin of the frustration determines the phase behaviour. Further SANS studies would be required to check this assumption. Some other experimental findings indicate already that the packing of the mesogenic cores in polyacrylates —the flexibility of which is intermediate between that of methacrylates and siloxanes— is highly influenced by the backbone conformations. For example, for some cyano-terminated polyacrylates the enthalpy of the smectic-isotropic transition decreases with increasing molar mass [28,29], in contrast to polysiloxanes where no such dependency is found [28].

Within the framework sketched above, we come to the following qualitative picture of the phase transformations in PABB-5. At high temperatures and large chain length the backbone is on average perpendicular to the side groups, stabilizing the nematic and Sm-A_d phases. Upon further cooling the prolate form of the backbone develops. From the packing point of view, it seems difficult to impose a smectic density modulation upon a configuration in which the backbone is nearly parallel to the director. The changing of preferential conformations of the backbone from oblate to prolate leads to an increase of the density of layer crossings by the polymer chain. Hence the changing anisotropy of the backbone conformation destabilizes the smectic layering and the Sm-A_d phase melts into the re-entrant nematic phase. Upon further cooling the $\tilde{C}$ phase condenses, in which the monoclinic 2D structure can more easily accommodate the prolate backbone configuration than the Sm-A_d structure (compare Fig. 7). However, the entropy cost of the steric mismatch induced by the prolate backbone conformation is still high and makes the $\tilde{C}$ phase rather defective. In this picture the frustration in the system is due to the conformation-density coupling. In agreement with this view, the Sm-A_d cannot exist at a low degree of polymerisation, where the prolate backbone conformation is dominant [30].

In conclusion, we have presented X-ray diffraction data that give evidence of a new type of frustrated phase diagram in side-chain LC polymers, which is driven by the

length of the polymer chain. The observations indicate a strong influence of the polyacrylate backbone conformations on the packing of the mesogenic side groups and thus on the thermodynamic stability of the various LC phases. The frustrated behaviour has a steric origin and is attributed to a coupling between the backbone conformations and the smectic density modulation. In the absence of a more complete microscopic understanding of LC polymers, we postulate a change from an oblate to a prolate backbone conformation to account for the various LC phase transitions at high and low degrees of polymerisation. A more quantitative connection with competing order parameter theories incorporating also the difference between monodisperse and polydisperse samples, remains an important challenge in the field of LC polymers.

The authors wish to thank A.I. Alexandrov, S. Diele, A.R. Khokhlov and B. Mulder for valuable discussions. This work is part of the research program of the "Stichting voor Fundamenteel Onderzoek der Materie, (FOM)", which is financially supported by the "Nederlandse Organisatie voor Wetenschappelijk Onderzoek, (NWO)". B.I.O. and S.N.S. acknowledge support from NWO in the framework of the cooperation program with the Russian Federation. We also acknowledge support from Russian Fund for Fundamental Research (under grant 00-03-33174).

References

1. See, for example, N.A. Plate (Editor), *Liquid-Crystal Polymers* (Plenum, New York, 1993); C.B. McArdle (Editor), *Side Chain Liquid Crystal Polymers* (Glasgow, Blackie, 1989).
2. H. Finkelmann, H. Ringsdorf, J.H. Wendorf, Macromol. Chem. **179**, 273 (1978); Ya.S. Freidzon, V.V. Tsukruk, N.I. Boiko, V.P. Shibaev, V.V. Shilov, Yu.S. Lipatov, Polymer Commun. **27**, 190 (1986); P. Davidson, A.M. Levelut, Liq. Cryst. **11**, 469 (1992); G. Sigaud, *Phase Transitions in Liquid Crystals*, edited by S. Martelucci, A.N. Chester (Plenum, New York, London, 1992) p. 37; P. Davidson, K. Kühnpast, J. Springer, G. Scherowsky, Liq. Cryst. **14**, 901 (1993).
3. R.G. Kirste, H.G. Ohm, Macromol. Chem. Rapid Commun. **6**, 179 (1985); P. Keller, B. Carvalko, J.P. Cotton, M. Lambert, F. Moussa, G. Pepy, J. Phys. Lett. **46**, 1065 (1985).
4. L. Noirez, P. Keller, P. Davidson, F. Hardouin, J.P. Cotton, J. Phys. **49**, 1993 (1988); L. Noirez, P. Davidson, W. Schwarz, G. Repy, Liq. Cryst. **16**, 1081 (1994); L. Noirez, C. Boeffel, A. Daoud-Aladine, Phys. Rev. Lett **80**, 1453 (1998).
5. W. Renz, M. Warner, Phys. Rev. Lett. **56**, 1268 (1986); A.B. Kunchenko, D.A. Svetogorsky, J. Phys. **47**, 2015 (1986); X.J. Wang, M. Warner, J. Phys. A **20**, 713 (1987); J. Rieger, J. Phys. **49**, 1615 (1988); J. Rieger, Liq. Cryst. **5**, 1559 (1989); W. Renz, Mol. Cryst. Liq. Cryst. **155**, 549 (1988).
6. A.N. Semenov, A.R. Khokhlov, Sov. Phys. Usp. **31**, 988 (1988).
7. V. Shibaev, Mol. Cryst. Liq. Cryst. **243**, 201 (1994); B.I. Ostrovskii, S.N. Sulyanov, N.I. Boiko, V.P. Shibaev, Liq. Cryst. **25**, 153 (1998).
8. N.I. Boiko, V.P. Shibaev, B.I. Ostrovskii, S.N. Sulyanov, D. Wulff, J. Springer, Macromol. Chem. Phys. **202**, 297 (2001).
9. See, for example, G. Aeppli, S.M. Shapiro, R.J. Birgeneau, H.S. Chen, Phys. Rev. B **28**, 5160 (1983) and references therein.
10. E.D. Specht, M. Sutton, R.J. Birgeneau, D.E. Moncton, P.M. Horn, Phys. Rev. B **30**, 1589 (1984); R.J. Birgeneau, P.M. Horn, Science **232**, 329 (1986).
11. P.E. Cladis, Phys. Rev. Lett. **35**, 48 (1975); D. Guillon, P.E. Cladis, J. Stamatoff, Phys. Rev. Lett. **41**, 1598 (1978).
12. See, for some reviews: F. Hardouin, A.M. Levelut, M.F. Achard, G. Sigaud, J. Chim. Phys. **80**, 53 (1983); P.E. Cladis, Mol. Cryst. Liq. Cryst. **165**, 85 (1988); R. Shashidhar, B.R. Ratna, Liq. Cryst. **5**, 421 (1989); B.I. Ostrovskii, *Structure and Bonding*, *Liquid Crystals I*, edited by D.M.P. Mingos, Vol. **94** (Springer, New York, Heidelberg, 1999) p. 199.
13. G. Pelzl, I. Latif, S. Diele, M. Novak, D. Demus, H. Sackmann, Mol. Cryst. Liq. Cryst. **139**, 353 (1986).
14. G. Sigaud, F. Hardouin, M. Mauzac, N.H. Tinh, N.H., Phys. Rev. A **33**, 789 (1986).
15. L. Longa, W.H. de Jeu, Phys. Rev. A **28**, 2380 (1983).
16. J. Prost, P. Barois, J Chim. Phys. **80**, 53 (1983); P. Barois, J. Pommier, J. Prost, *Solitons in Liquid Crystals*, edited by L. Lam, J. Prost (Springer, Berlin, 1992) Chapt. 6.
17. J.O. Indekeu, A.N. Berker, Phys. Rev. A **33**, 1158 (1986); R.R. Netz, A.N. Berker, Phys. Rev. Lett. **68**, 333 (1992).
18. F. Hardouin, N.H. Tinh, M.F. Achard, A.M. Levelut, J. Phys. Lett. **43**, 327 (1982); E. Fontes, P.A. Heiney, J.L. Haseltine, A.B. Smith, J. Phys. **47**, 1553 (1986); T.A. Lobko, B.I. Ostrovskii, W. Haase, J. Phys. II **2**, 1195 (1992); Y.Shi, G. Nounesis, S. Kumar, Phys. Rev. E **54**, 1570 (1996).
19. H. Stevens, G. Rehage, H. Finkelmann, Macromolecules **17**, 851 (1984); V.P. Shibaev, N.A. Plate, Pure & Appl. Chem. **57**, 1589 (1985); T.I. Gubina, S. Kise, S.G. Kostromin, R.V. Talrose, V.P. Shibaev, N.A. Plate, Liq. Cryst. **4**, 197 (1989); Ya. S. Freidzon, N.I. Boiko, V.P. Shibaev, N.A. Plate, Dokl. Akad. Nauk. USSR **308**, 1419 (1989); V. Percec, B.Hahn, Macromolecules **22**, 1588 (1989); V.P. Shibaev, Ya. S. Freidzon, S.G. Kostromin, *Liquid Crystalline and Mesomorphic Polymers*, edited by V.P. Shibaev, L. Lam (Springer, New York, 1994) Chapt. 3.
20. S.N. Sulianov, A.N. Popov, D.M. Kheiker, J. Appl. Cryst. **27**, 934 (1994).
21. E.A.L. Mol, J.D. Shindler, A.N. Shalaginov, W.H. de Jeu, Phys. Rev. E **54**, 536 (1996).
22. See, for example, B.E.Warren, *X-ray Diffraction* (Dover, New York, 1990).
23. P.S. Pershan, J. Prost, J. Phys. Lett. **40**, L-27 (1979).
24. R.M. Richardson, E.B. Barmatov, I.J. Whitehouse, V.P. Shibaev, T. Yongjie, M.H.F. Godinho, Mol. Cryst. Liq. Cryst. **330**, 285 (1999).
25. C. Boeffel, H.W. Spiess, B. Hisgen, H. Ringsdorf, H. Ohm, R.G. Kirste, Macromol. Chem. Rapid Commun. **7**, 777 (1986).

26. L. Benguigui, L. Noirez, R. Kahn, P. Keller, M. Lambert, E. Cohen de Lara, J. Phys. II **1**, 451 (1991).
27. W.G. Bouwman, W.H. de Jeu, Liq. Cryst. **16**, 863 (1994).
28. V. Percec, M. Lee, Macromolecules **24**, 1017 (1991).
29. U.W. Gedde, H. Jonsson, A. Hult, V. Percec, Polymer **33**, 4352 (1992).
30. As suggested by one of the referees, an alternative explanation could be found in the spatial distribution of the portions of the backbone that are nearly parallel to **n**. In particular, the regions where the backbone crosses the layers could be randomly distributed in the Sm-A_d phase and periodically distributed in the $\tilde{C}$ phase. The pattern from Figure 6 then could be considered as the product of the form factor of isolated crossing defects (cf. P. Davidson, A.M. Levelut, J. Phys. **49**, 689 (1988)) and the interference function of the 2D lattice.